

Imaging of tumor angiogenesis in rat brains *in vivo* by photoacoustic tomography

Geng Ku, Xueding Wang, Xueyi Xie, George Stoica, and Lihong V. Wang

Green laser pulses at a wavelength of 532 nm from a Q-switched Nd:YAG laser were employed as irradiation sources for photoacoustic tomography (PAT). The vascular structure of the brain was imaged clearly, with optimal contrast, because blood has strong absorption near this wavelength. The photoacoustic images of rat brain tumors in this study clearly reveal the angiogenesis that is associated with tumors. Brain tumors can be identified based on the distorted vascular architecture of brain tumorigenesis and related vascular changes, such as hemorrhage. This research demonstrates that PAT can potentially provide a powerful tool for small-animal biological research. © 2005 Optical Society of America

OCIS codes: 170.5120, 170.3880, 170.0110.

1. Introduction

Photoacoustic tomography (PAT) is a nonionizing imaging modality for visualizing biological tissues with high optical contrast and high ultrasonic resolution. PAT is based on the measurement of laser-induced ultrasonic waves. This imaging modality has contrast similar to that of pure optical imaging and spatial resolution similar to that of pure ultrasonic imaging. Therefore PAT combines the advantages of two imaging modalities in a single modality.

The laser-induced ultrasonic signals from a biological sample depend on the optical absorption in the sample to reveal the structure of the tissues based on optical contrast. Under illumination by green laser light at a wavelength of 532 nm, the optical absorption of whole blood is much stronger than that of other tissues: The absorption coefficient of human blood at this wavelength is nearly 200 cm^{-1} , which is almost 10 times higher than that of epidermis and nearly 500 times higher than that of dermis.¹ Therefore blood generates strong photoacoustic signals and

manifests high image contrast, causing the vasculature in organs to stand out prominently in photoacoustic images. Besides optical absorption, the thermal and elastic properties of the tissues also affect the strength of photoacoustic signals. Therefore physical changes, such as density in a tissue, can be reflected in photoacoustic images. The increased density of tumor-bearing tissues is most likely due to a passive mechanism referred to as the enhanced permeability and retention effect.² In this paper, however, we focus solely on the optical contrast that is due to high hemoglobin absorption.

The arrangement of the ultrasonic detector(s) about the region of interest determines the imaging mode and the reconstruction algorithm. For *in vivo* detection of tissue structures under the skin, the ultrasonic transducer can be placed, or scanned, on the skin.^{3,4} Hoelen and de Mul achieved photoacoustic imaging of vasculature by employing a planar scan of an ultrasonic transducer.⁵ Their images, which were reconstructed by use of a delay-and-sum algorithm, presented depth resolution better than $20 \mu\text{m}$ and lateral resolution better than $200 \mu\text{m}$. A single focused ultrasonic transducer can provide one-dimensional images along the ultrasonic axis, and scanning the transducer linearly over a sample can provide two-dimensional images. In this imaging configuration, the image resolutions are determined by the focal parameters and the bandwidth of the ultrasonic detection system that is employed.^{6,7} Recently, Kolkman *et al.*⁸ developed a double-ring detector, which improved the detection directivity, to image veins proximal to the wrist in humans. The feasibility

G. Ku (gku@oilab.tamu.edu), X. Wang, X. Xie, and L. V. Wang (LWang@tamu.edu) are with the Optical Imaging Laboratory, Department of Biomedical Engineering, Texas A&M University, 3120 TAMU, College Station, Texas 77843-3120. G. Stoica is with the Department of Pathobiology, Texas A&M University, College Station, Texas 77843-5547.

Received 19 July 2004; revised manuscript received 7 October 2004; accepted 20 October 2004.

0003-6935/05/050770-06\$15.00/0

© 2005 Optical Society of America

of imaging small, deeply embedded tumors was also studied by Esenaliev *et al.*, who used tissue phantoms.⁹ Oraevsky *et al.* used photoacoustic imaging to detect ductal–lobular carcinoma in the human breast.¹⁰ Using a single ultrasonic transducer to scan circularly about a small-animal head, Wang *et al.*^{11,12} and Ku *et al.*¹³ reconstructed clear photoacoustic images of the cortical vasculature in the brain *in vivo* with high spatial resolution and high optical contrast.

Studies in oncology have shown that angiogenesis, which refers to the formation of new blood vessels within a tumor or the growth of blood vessels between a tumor and its surrounding tissues, plays an important role in tumor growth and metastasis.¹⁴ Angiogenesis constitutes an important control point in the progression of cancer. It has also been proposed that the low metastatic activity of some *in situ* tumors may be related to the inability of these tumors to form these new vessels.^{15,16} There is continued interest in the development of *in vivo* animal models of brain metastasis to help further the understanding of the mechanisms that underlie the spread of tumors and to develop more-effective therapies. Unique anatomical and physiological properties of the brain may require special considerations for the design of effective therapies for use against metastases in this organ. Brain metastatic cells may be sheltered from the effects of some therapeutic agents or immune effector cells by the blood–brain barrier or by specific properties of the brain’s microenvironment. Furthermore, some of the consequences of treatment-related complications, such as edema and hemorrhage, are more serious in the brain than in other organs. Based on these specific peculiarities of the brain, a noninvasive imaging modality such as PAT is desirable to permit continuous monitoring of the dynamics of the metastatic process and of a tumor’s therapeutic paradigm in the same animal.

In this paper we demonstrate both *ex vivo* and *in vivo* photoacoustic imaging of brain tumors associated with angiogenesis in a rat animal model. The imaged vasculature is underneath the scalp and skull, within a few millimeters from the laser-illuminated surface. All the photoacoustic images are compared with photographs or the histology of the samples, which were taken after the photoacoustic imaging. To acquire high-quality images with spatial resolutions of various scales, we employed multiple ultrasonic transducers of different bandwidths to scan the rat brain simultaneously and then reconstructed the images by using the data acquired through each transducer independently. The photoacoustic images of both the normal vasculature and the tumor angiogenesis detected by the different bandwidths are compared.

2. Experimental Setup

The experimental setup of PAT for rat brain tumor detection is shown in Fig. 1. The laser light at a wavelength of 532 nm from a Q-switched Nd:YAG laser (Brilliant B, BigSky), operating at the second

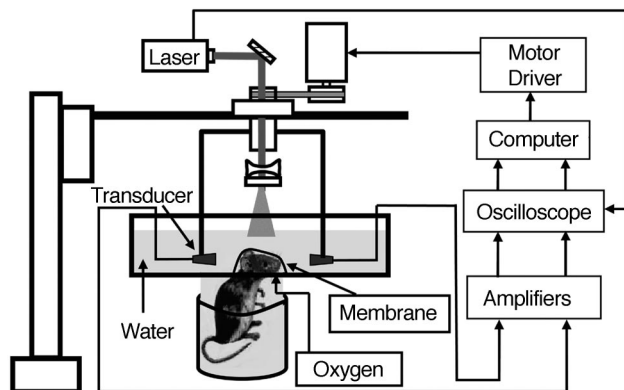


Fig. 1. Experimental setup of PAT for rat tumor imaging.

harmonic wave, is employed as the irradiation source. The laser pulse width is 6.5 ns, and the pulse repetition rate is 10 Hz. The laser beam is expanded by a concave lens and homogenized by a ground glass to illuminate the rat head from its top. The pulse energy density on the sample surface is controlled to ~ 20 mJ/cm², which is the “maximum permissible exposure” for human skin at a wavelength of 532 nm, according to the ANSI standard.¹⁷

The photoacoustic system has three detection channels that can receive photoacoustic signals through three ultrasonic transducers independently. The ultrasonic transducers (V383, XMS-310, and V316-N; Panametrics) have central frequencies of 3.5, 10, and 20 MHz, respectively. The nominal bandwidths of these three transducers are 50–80% of their central frequencies. The diameters of the active areas are 10, 2, and 3 mm for the 3.5-, 10-, and 20-MHz transducers, respectively. The spatial resolution within the imaging plane appeared to be approximately 210, 60, and 30 μ m for the 3.5-, 10-, and 20-MHz transducers, respectively.¹³ The transducers convert the laser-induced photoacoustic energy into electrical signals. The electrical signals are amplified by amplifiers (ZFL-500LN; Mini-Circuits) and filtered by homemade filters that correspond to the central frequencies and bandwidths of the ultrasonic transducers. An oscilloscope with four channels (TDS-540A; Tektronix) is employed to digitize the three channels of photoacoustic signals simultaneously. A LabView program controls the laser firing, the scanning of the transducers, and the data acquisition.

Each transducer is mounted upon a post and connected to a rotational apparatus such that circular scanning in the horizontal plane about the sample can be implemented. The rotational apparatus mounted upon a bearing is driven by a step motor (MD-2; Arrick Robotics). The normal of the active surface of the ultrasonic transducer is aligned perpendicularly to the rotational axis of the circular scanning. We typically complete a full view of a 2π circular scan with 240 steps (1.5°/step). The entire horizontal scanning section is connected to an upright translation stage. Hence this section of the sys-

tem can be manually adjusted vertically to align the scanning plane with the cross section of interest.

For coupling the photoacoustic signals from the sample to the ultrasonic transducer, the transducers are immersed in a tank of water. The rat head is allowed to protrude into the water tank through a hole in the bottom of the tank and is insulated from the water by a piece of clear polyethylene membrane covering the hole. Sprague Dawley rats of 100–200-g body weight are employed in the imaging experiment. General anesthesia is administered to the rat by an intramuscular injection of a mixture of ketamine hydrochloride (44 mg/kg), xylazine hydrochloride (2.5 mg/kg), acepromazine maleate (0.75 mg/kg), and atropine (0.025 mg/kg). The initial anesthesia is maintained as required with an additional half-dose of the intramuscular agents. During the procedure the rat is placed on a water-circulating heating pad (Gaymar T/pump, Gaymar Industries), and additional heat is provided by an overhead surgical lamp. Before the photoacoustic imaging, the hair on the rat's head is removed gently with hair-remover lotion. During the data acquisition, pure oxygen is provided to the rat for breathing, and its arterial blood oxygenation (SpO_2) level and heart rate are monitored by a pulse oximeter (8600V; Nonin) with the fiber-optic probe wrapped around the rat's paw. The SpO_2 level was near 90% and the heart rate was close to 350 beats/min throughout the experiment, which shows that the rat was in good condition.

To perform the PAT imaging we used a rat animal model that was previously developed by Hall and Stoica.¹⁸ The applied rat mammary adenocarcinoma cell line (*Br7-C5*) preferentially metastasizes to the brain when the tumor cells are inoculated via the left ventricle (10^6 cells in 0.2 mL of cultured media). Tumor cells are also transcranially implanted (orthotropic inoculation, 10^5 monodispersed cells) into the brain cortex. One month after the intracerebral inoculation, the experimental rat develops a tumor nodule (~ 0.5 cm in diameter) on the cortical surface of the brain, which often protrudes through the skull. The left heart ventricle of the inoculated rat develops neurological clinical signs 40 days postinoculation owing to the development of brain metastases. A histological examination demonstrates that brain metastases are multifocally disseminated within the brain. The inoculation procedures are performed under anesthesia with the ketamine cocktail described above.

3. Results and Discussion

Photoacoustic images of a tumor-bearing rat brain are acquired *ex vivo* (Fig. 2) with the rat's scalp removed. At the bottom of Fig. 2(a) an open-skull photograph of the rat brain shows a tumor in the cerebellum. The tumor area at the top left of the photograph appears darker than the other parts of the brain cortex. A vibrotome histological section of the tumor, which illustrates tumor hypercellularity and an abundant array of tortuous irregular dis-

torted vessels, is shown at the top of Fig. 2(a). The photoacoustic images of the rat cerebellum detected by the 3.5- and 10-MHz transducers are shown in Figs. 2(b) and 2(c), respectively: The global images of the brain are shown at the bottom, and the corresponding close-up images of the tumor are shown at the top. In previous PAT experiments, photoacoustic images of tumor-free brains showed well-defined symmetrical vascular architecture in both cortical hemispheres. We believe that the detected photoacoustic signals originate primarily from superficial cerebral veins, sagittal sinus veins, transverse sinus veins and their tributaries, and tumor neovascularization. In a comparison of the photograph with the photoacoustic images shown in Fig. 2, PAT reveals the vascular architecture associated with the tumorigenesis, which is different from that of a normal brain image. The well-vascularized tumor in the photoacoustic images exhibits dense dark spots or stripes that represent strong photoacoustic sources from the irregular vessels of angiogenesis, in which the hemoglobin strongly absorbs the laser light. In other words, the normal vascular architecture in the tumor-occupied area is replaced by the newly formed irregular and distorted vessels. The density of the capillaries in the tumor area is also higher than in the normal brain. In summary, tumors exhibit two obvious peculiarities in their vascular structures in the photoacoustic images: a distorted irregular vascular system and an increased density of vessels. The histology confirms that the cerebellar tumor is well vascularized and the presence of a hemorrhagic parenchyma. Both of these factors lead to an increased hemoglobin concentration and subsequently to strong photoacoustic signals.

The photoacoustic images acquired with the 3.5- and 10-MHz transducers both show the main vasculature and vessel ramifications with good image quality but with different spatial resolutions. The photoacoustic signal detected by the 3.5-MHz transducer is stronger; consequently, the corresponding image has a better signal-to-noise ratio, and the vascular structure looks more obvious. The image acquired with the 10-MHz transducer has higher image resolution, and the subtle vessels are more distinct. Although angiogenesis and distorted vasculature are evident in both the histology and the close-up photoacoustic images, the geometrical shapes of the vessels in the histology differ from those in the photoacoustic images for the following two reasons: First, the orientations of the histologic cross section and the imaged layer are not identical. Second, the histology is from a 5- μm -thick cross section of the rat brain, whereas the photoacoustic images are from a layer of ~ 4 mm thickness.¹³

Figure 3 presents an *in vivo* photoacoustic image of the brain of a living rat with a tumor on its left frontal hemisphere. The image was noninvasively acquired with a 10-MHz ultrasonic transducer. The original photoacoustic image is shown at the left in Fig. 3, and a close-up image of the tumor area is shown at the bottom right. After the experiment, the rat was sac-

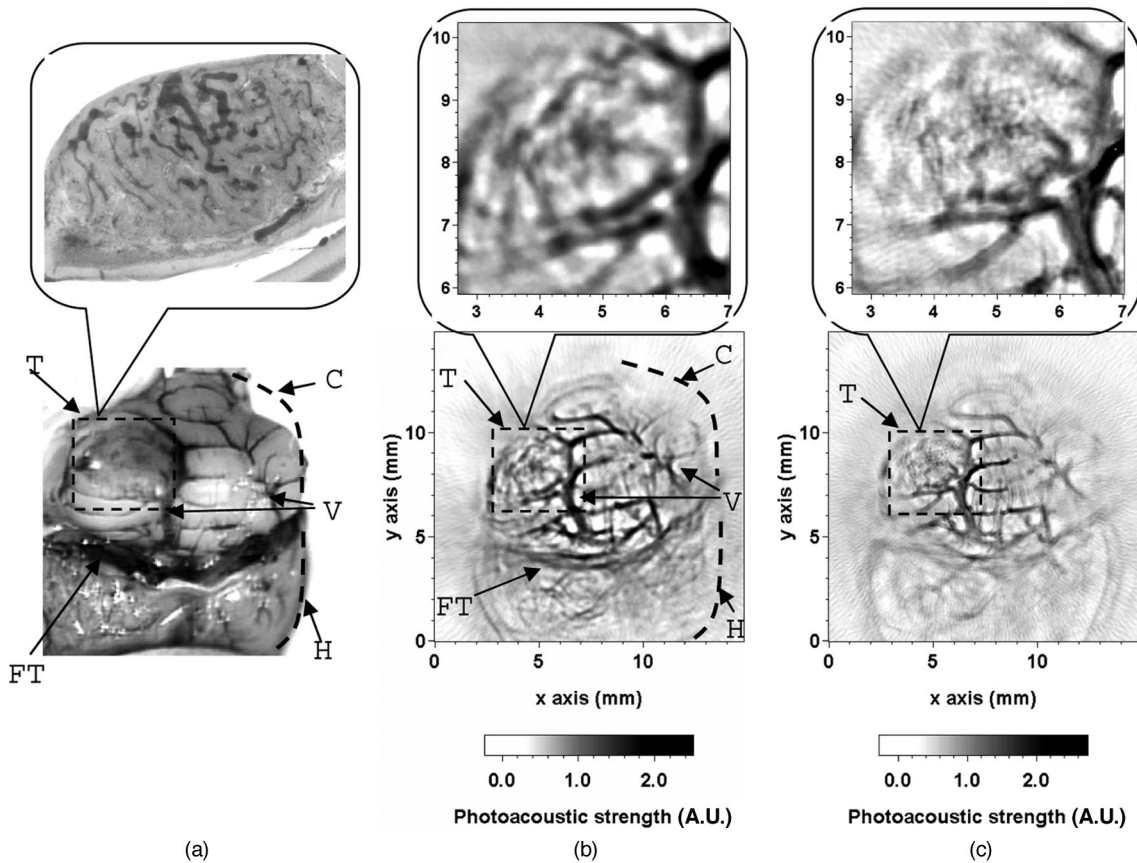


Fig. 2. Comparison of a photograph of a tumor-bearing rat brain and several photoacoustic images. (a) Bottom, photograph of the open-skull rat brain, showing a tumor in its cerebrum; top, histology of the cerebellar tumor. T, tumor; FT, fissure transversa; C, cerebellum; V, blood vessels; H, partial view of the cerebral hemisphere. Photoacoustic images of the rat brain and close-up images of the tumor acquired with (b) a 3.5-MHz ultrasonic transducer and (c) a 10-MHz ultrasonic transducer.

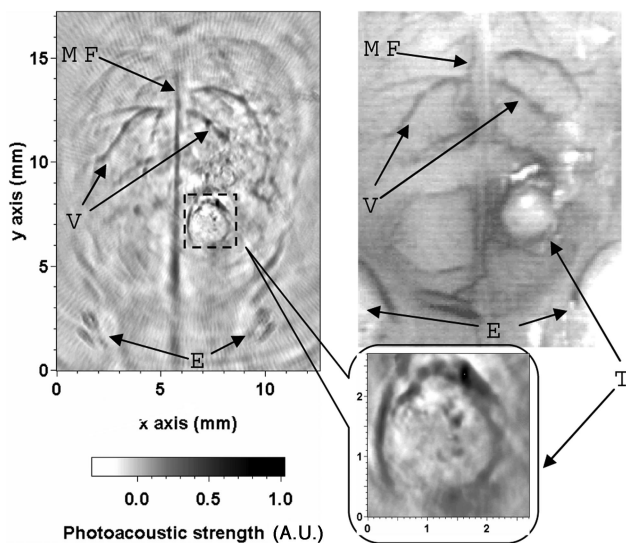


Fig. 3. Left, *in vivo* photoacoustic image of a rat brain containing a tumor in its left cerebral hemisphere cortex acquired with a 10-MHz ultrasonic transducer. Bottom right, close-up photoacoustic image of the tumor. Top right, photograph of the rat brain through the skull where the scalp was stripped after photoacoustic imaging. MF, median fissure; V, blood vessels; T, tumor; E, eyes.

rified and its scalp stripped for comparison of the anatomy of the rat brain (shown at the top right in Fig. 3) with the photoacoustic images. The tumor-associated vasculature distortion can easily be recognized on the photoacoustic image. In the tumor-free area of the brain cortex, the vessel branches exhibit a normal distribution. However, in the tumor area, the normal vascular architecture is seriously distorted by the growing new blood vessels. The close-up image of the tumor area clearly shows the vascular distortion inside and around the tumor. The abnormal vessels that were owing to angiogenesis surround and feed the tumor. This type of tumoral vascular structure under the skin and skull can be clearly imaged non-invasively by PAT.

Figures 4(a) and 4(b) show two *in vivo* photoacoustic images, acquired noninvasively with the 3.5- and 20-MHz ultrasonic transducers, respectively, of the brain of another living rat with tumors in its left frontal hemisphere. Two close-up photoacoustic images of the tumors are shown in Fig. 4 as well. The images are compared with the open-skull photograph of the rat brain [Fig. 4(c)], which was taken after the photoacoustic imaging experiment. In the left frontal hemisphere the normal vascular distribution was seriously distorted. Besides the tumor-associated

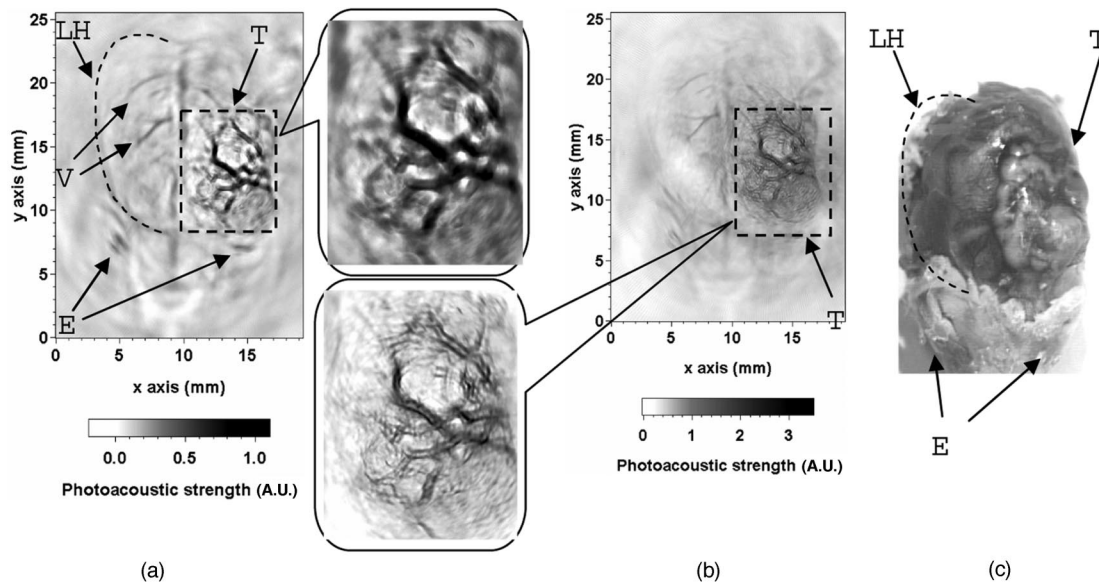


Fig. 4. *In vivo* photoacoustic images and close-ups of a rat brain with tumors in the left cerebral hemisphere acquired with (a) a 3.5-MHz ultrasonic transducer and (b) a 20-MHz ultrasonic transducer. (c) Photograph of the rat brain through the skull where the scalp was stripped after photoacoustic imaging. LH, left cerebral hemisphere; V, blood vessels; E, eyes; T, tumor.

irregular and distorted vessels, the hemorrhagic infiltration of the parenchyma is more evident in the tumor area of this rat. Because vessels in developing tumors are more permeable than those in normal tissue, blood can leak into the tumor's parenchyma, which also contributes to an increase in optical absorption in the tumor. We attribute the observed photoacoustic imaging patterns to the leaky nature of the tumor vessels, which contain wide interendothelial junctions, an incomplete or absent basement membrane, and large numbers of transendothelial channels.^{19,20} The photoacoustic images acquired with both the 3.5- and the 20-MHz transducers disclose the distorted vasculature associated with the tumorigenesis, but the two images present different characteristics. In the close-up image acquired with the 3.5-MHz transducer, the vessels exhibit solid, blurred contours, whereas in the close-up image acquired with the 20-MHz transducer the vessel contours are better delineated.

4. Conclusion

Photoacoustic tomography can be used to detect tumors in rat brains by imaging of the tumor-related vasculature and the tumor's parenchymal imbibition of blood. The image resolution and contrast are good enough to resolve the vessels in the brain; therefore a tumor associated with angiogenesis can be diagnosed reliably. PAT is suitable for monitoring tumor growth, angiogenesis, and antiangiogenic therapy in experimental carcinogenesis on animal models. This noninvasive technology allows for monitoring the same animal at multiple times as well as reducing the individual variability and the number of experimental animals required.

This study is sponsored by the National Institutes of Health (grants R01 NS46214-01 and R01 EB000712).

References

1. S. L. Jacques and S. A. Prahl, "Absorption spectra for biological tissues," (Oregon Medical Laser Center, Portland, Oreg., 2004), <http://omlc.ogi.edu/classroom/ece532/class3/muaspectra.html>.
2. H. Maeda, "The enhanced permeability and retention (EPR) effect in tumor vasculature: the key role of tumor-selective macromolecular drug targeting," *Adv. Enzyme Regul.* **41**, 189–207 (2001).
3. A. A. Karabutov, E. V. Savateeva, N. B. Podymova, and A. A. Oraevsky, "Backward mode detection of laser-induced wide-band ultrasonic transients with optoacoustic transducer," *J. Appl. Phys.* **87**, 2003–2014 (2000).
4. A. A. Karabutov, E. V. Savateeva, and A. A. Oraevsky, "Imaging of layered structures in biological tissues with optoacoustic front surface transducer," in *Laser-Tissue Interaction X: Photochemical, Photothermal, and Photomechanical*, S. L. Jacques, G. J. Mueller, A. Roggan, and D. H. Sliney, eds., *Proc SPIE* **3601**, 284–295 (1999).
5. C. G. A. Hoelen and F. F. M. de Mul, "Image reconstruction for photoacoustic scanning of tissue structures," *Appl. Opt.* **39**, 5872–5883 (2000).
6. G. Ku and L.-H. V. Wang, "Scanning thermoacoustic tomography in biological tissue," *Med. Phys.* **27**, 1195–1202 (2000).
7. G. Ku and L.-H. V. Wang, "Scanning microwave-induced thermoacoustic tomography: signal, resolution, and contrast," *Med. Phys.* **28**, 4–10 (2001).
8. R. G. M. Kolkman, J. H. G. M. Klaessens, E. Hondebrink, J. C. W. Hopman, F. F. M. de Mul, W. Steenbergen, J. M. Thijssen, and T. G. van Leeuwen, "Photoacoustic determination of blood vessel diameter," *Phys. Med. Biol.* **49**, 4745–4756 (2004).
9. R. O. Esenaliev, A. A. Karabutov, and A. A. Oraevsky, "Sensitivity of laser optoacoustic imaging in detection of small

- deeply embedded tumors," *IEEE J. Sel. Top. Quantum Electron.* **5**, 981–988 (1999).
10. A. A. Oraevsky, E. V. Savateeva, S. V. Solomatin, A. A. Karabutov, V. G. Andreev, Z. Gatalica, T. Khamapirad, and P. M. Henrichs, "Optoacoustic imaging of blood for visualization and diagnostics of breast cancer," in *Biomedical Optoacoustics III*, A. A. Oraevsky, ed., *Proc. SPIE* **4618**, 81–92 (2002).
 11. X. Wang, Y. Pang, G. Ku, X. Xie, G. Stoica, and L.-H. V. Wang, "Non-invasive laser-induced photoacoustic tomography for structural and functional imaging of the brain *in vivo*," *Nat. Biotechnol.* **21**, 803–806 (2003).
 12. X. Wang, G. Ku, M. A. Wegiel, D. J. Bornhop, G. Stoica, and L.-H. V. Wang, "Noninvasive photoacoustic angiography of animal brains *in vivo* with near-infrared light and an optical contrast agent," *Opt. Lett.* **29**, 730–732 (2004).
 13. G. Ku, X. Wang, X. Xie, G. Stoica, and L.-H. V. Wang, "Multiple-bandwidth photoacoustic tomography," *Phys. Med. Biol.* **49**, 1329–1338 (2004).
 14. F. Judah, "Angiogenesis in cancer, vascular, rheumatoid and other disease," *Nat. Med. (N.Y.)* **1**, 27–31 (1995).
 15. P. Carmeliet, K. Rakesh, and R. K. Jain, "Angiogenesis in cancer and other diseases," *Nature* **407**, 249–257 (2000).
 16. F. Judah, "Role of angiogenesis in tumor growth and metastasis," *Semin. Oncol.* **29**, 15–18 (2002).
 17. American National Standards Institute, *American National Standard for the Safe Use of Lasers ANSI Z136.1-2000* (American National Standards Institute, New York, 2000).
 18. G. D. Hall and G. Stoica, "Characterization of brain and bone-metastasizing clones selected from an ethylnitrosourea-induced rat mammary carcinoma," *Clin. Exp. Metast.* **12**, 283–295 (1994).
 19. H. Maeda, "The enhanced permeability and retention (EPR) effect in tumor vasculature: the key role of tumor-selective macromolecular drug targeting," *Adv. Enzyme Regul.* **41**, 189–207 (2001).
 20. H. Maeda, J. Fang, T. Inutsuka, and Y. Kitamoto, "Vascular permeability enhancement in solid tumor: various factors, mechanisms involved and its implications," *Int. Immunopharmacol.* **3**, 319–328 (2003).